Capacitive Touch Systems With Styli for Touch Sensors: A Review

Oh-Kyong Kwon, *Member, IEEE*, Jae-Sung An, *Student Member, IEEE*, and Seong-Kwan Hong, *Member, IEEE*

***Abstract*— This paper presents the latest progress in development and applications of the capacitive touch systems (CTSs) with styli. The CTSs, which include the touch sensor, analog front-end (AFE) integrated circuit (IC), and micro-controller unit, are reviewed along with the passive and active styli. The architecture of the CTS is explained first, followed by an exploration of the touch sensors: (1) types of touch sensors, such as in-cell, on-cell, and add-on types according to the size and material, (2) AFE IC with the driving and sensing methods, and (3) passive and active styli for the CTS. Finally, the future perspectives of the CTS are given from the viewpoint of the technical developments.**

***Index Terms*— Analog front-end (AFE) IC, stylus, touch sensor, capacitive touch system (CTS).**

I. Introduction

AMONG the various touch systems such as acoustic [1]–[7], near-infrared [8]–[11], resistive [12]–[15], and capacitive types [16]–[50], capacitive touch systems (CTSs) are widely used in many applications such as smart watches, mobile phones, desktop PCs, and interactive white boards due to their multi-touch capability, durability, and high sensitivity [16]–[94].

Fig. 1 shows the classification of the types of touch sensors, the analog front-end (AFE) integrated circuit (IC) with driving and sensing methods, and the passive and active styli in CTSs. The touch sensors are classified into the add-on, on-cell, and in-cell types according to their location on or in the display panel as shown in Fig. 1(a) [18], [29], [36]. The add-on type [18] is easily implemented in the CTS because the touch sensor is attached on the display panel with an air gap. However, it has high thickness, heavy weight, high manufacturing cost, and low transmittance. The on-cell type [29] has no air gap because the touch sensor is located between the display cover glass and a display device in the display panel. Thus, it has higher transmittance, lower manufacturing cost, less weight, and thinner thickness than the add-on type. However, the touch sensor is located far from the finger and near to the display driver IC (DDI), thus generating a less capacitance variation and a larger display noise, respectively, resulting in a lower signal-to-noise (SNR) than the add-on type. The in-cell type [36] integrates the touch sensor on the display device in the display panel, thus having less weight, less thickness, and lower manufacturing cost than the add-on and on-cell types. However, the touch sensor is located far from the finger and nearer to the DDI than the on-cell and add-on types, thus degrading the SNR.

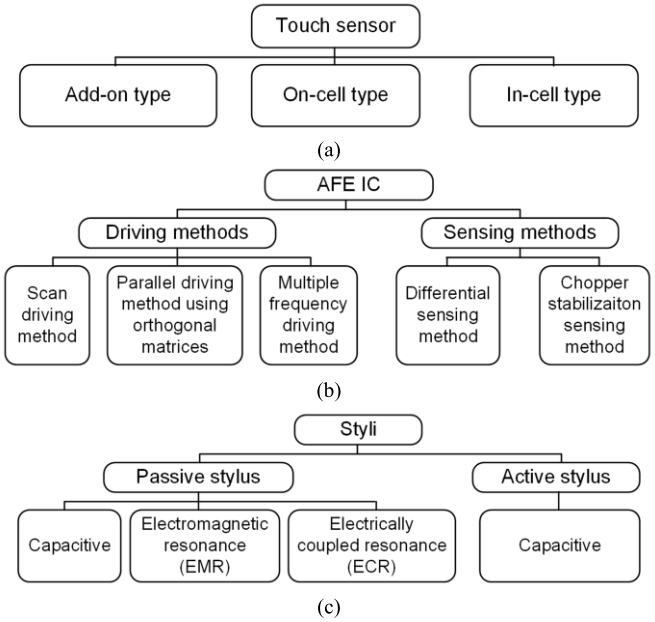

Fig. 1. Classification of (a) types of touch sensors, (b) AFE IC with driving and sensing methods, and (c) passive and active styli.

The AFE ICs generally need to sense small capacitance variation under the noisy environment and respond to the fast movement of the finger or styli. To satisfy the aforementioned demands, an AFE IC with various driving and sensing methods has been researched [16]–[71].

The driving methods are classified into the scan driving method (SDM), parallel driving method (PDM), and multiple frequency driving method (MFDM) as shown in Fig. 1(b). In the SDM [16], the AFE IC sends the excitation signal (V_{EXT}) sequentially to the transmitter (TX) electrodes. This SDM can be simply implemented in the AFE IC, but the sensing time of each TX electrode decreases as the number of TX electrodes increases, thus decreasing the SNR and frame rate of the AFE IC. In the PDM [38], the AFE IC simultaneously sends the V_{EXT}s to all the TX electrodes using orthogonal matrices such as Walsh-Hadamard and maximum length sequences and detects the touch coordinates of all

Manuscript received March 6, 2018; revised April 13, 2018; accepted April 23, 2018. Date of publication April 26, 2018; date of current version May 22, 2018. The associate editor coordinating the review of this paper and approving it for publication was Dr. Ferran Reverter. *(Corresponding author: Oh-Kyong Kwon.)*

The authors are with the Department of Electronic Engineering, Hanyang University, Seoul 04763, South Korea (e-mail: okwon@hanyang.ac.kr).

Digital Object Identifier 10.1109/JSEN.2018.2830660

electrodes. Accordingly, the sensing time of each TX electrode using the PDM does not decrease as the number of TX electrodes increases, resulting in an increase in the sensing time compared to the SDM, and thus the AFE IC using the PDM achieves a high SNR. However, as the number of TX electrodes increases, the size of the orthogonal matrices also increases, thus decreasing the frame rate. In the MFDM [49], the AFE IC determines the frame rate according to the minimum frequency of V_{EXT}s instead of the number of TX electrodes, thus achieving a higher frame rate and higher SNR regardless of the size of the touch sensor.

The sensing methods are classified into differential and chopper stabilization sensing methods [51]–[71]. In the differential sensing method [51]–[66], the AFE IC sends the complementary V_{EXT}s to the two adjacent TX electrodes and senses the difference of charge signals (Q_Ss) between the two adjacent receiver (RX) electrodes. This method can be realized with a simple circuit structure in the AFE IC, but cannot effectively remove the external noise because the amplitudes of external noises at the RX electrode and the adjacent one are different. In the chopper stabilization sensing method [67]–[71], the AFE IC sends the V_{EXT}, whose frequency is apart from the frequency of external noises, and senses the induced Q_S from the single RX electrode of the touch sensor. Among the various touch sensors, the large-sized touch sensor has a wide electrode pitch, and thereby the amplitudes of the induced external noise between the two RX electrode are different. Therefore, the chopper stabilization sensing method is more suitable for the large-sized touch sensors. However, it is difficult to remove the external noises when the frequency of the touch signal is near to that of the external noises.

The styli [72]–[94] can be classified into passive and active styli depending on whether the battery is integrated into the stylus or not as shown in Fig. 1(c). In the passive stylus, the capacitive type [72] is predominantly used in the CTS due to its low manufacturing cost, but it has a low SNR and limited expressions. The electromagnetic resonance (EMR) type [73]–[76] stylus can express the pressure and tilt angle with a narrow tip, but requires an additional EMR sensor underneath the display panel, thus increasing the power consumption, manufacturing cost, and thickness. The electrically coupled resonance (ECR) type [77]–[79] stylus does not need an additional sensor, thus reducing the power consumption, manufacturing cost, and thickness, but only representing a pressure expression with low resolution. The active stylus [80]–[94] can represent various expressions such as pressure and tilt angle, but requires additional circuit and battery in the active stylus, thus increasing the thickness, power consumption, and manufacturing cost of the stylus.

This paper presents the latest progress in development and applications of the CTSs, which include touch sensor, AFE IC, and styli. Section II explains the system architecture of the CTS. Sections III and IV describe types of touch sensors, and the driving and sensing methods of the AFE IC, respectively. In Section V, stylus technologies for CTS are reviewed. Finally, future perspectives and conclusions are given in Sections VI and VII, respectively.

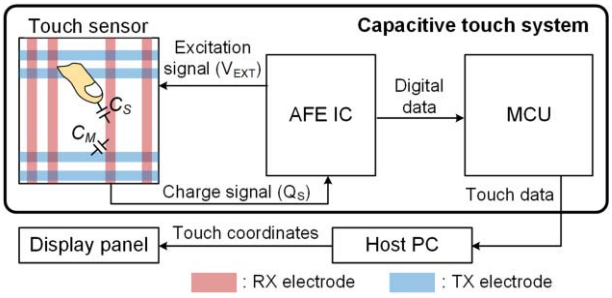

Fig. 2. System architecture of the capacitive touch system (CTS).

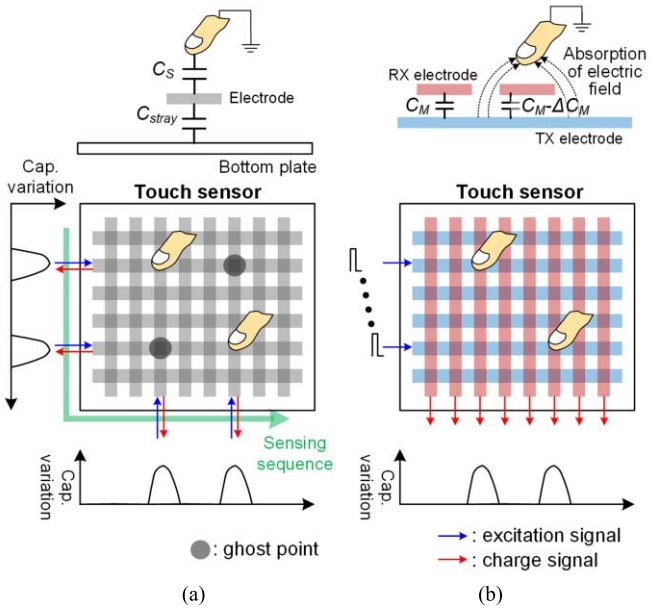

Fig. 3. (a) Self-capacitor (Cs) and (b) mutual-capacitor (C_M) sensing methods [16], [18], [22], [23], [34], [36], [42], [45], [46].

II. System Architecture of a Capacitive Touch System (CTS)

Fig. 2 shows the system architecture of the CTS, which includes the touch sensor, AFE IC, and MCU. When the AFE IC sends the V_{EXT} to the touch sensor, Q_S is induced into the AFE IC via self- or mutual-capacitors (C_Ss or C_Ms). The AFE IC converts the Q_S to the digital data and transfers it to the MCU. The MCU converts the digital data to the touch data for one frame time and transfers it to the host PC. The host PC then extracts the touch coordinate using the interpolation algorithms and sends it to the display panel [21], [37].

A. Self-Capacitor (C_S) Sensing Method

To sense the C_S or C_M, the AFE IC uses two sensing methods as shown in Fig. 3. Fig. 3(a) shows the C_S sensing method [34], [36], [46], [50], where the stray capacitor (C_{stray}) is defined by the capacitance between the electrode and bottom plate. When the finger touches the touch sensor, the C_S is formed between the finger and electrode. In the C_S sensing method, the AFE IC sequentially sends the V_{EXT}s to the electrodes and senses the Q_S at the same electrodes, thus sensing the variation in the C_S (ΔC_S) with C_{stray}.

TABLE I
TYPES OF TOUCH SENSOR

Types	ADD-ON [18], [22], [23], [25], [27]–[28], [30]–[31], [34]–[35], [38], [44]–[45], [47]–[49], [56]–[58]	On-cell [29], [46], [51], [59]–[60], [69]	In-cell [36], [39], [40]–[41], [50], [55]
Cross-sectional view of touch sensor and display panel[1]	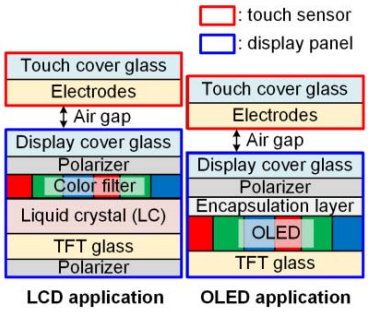	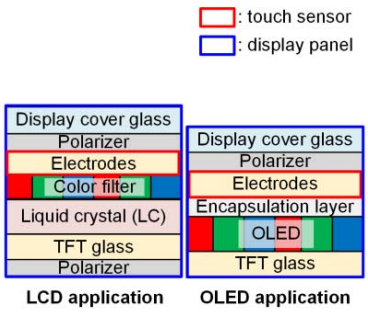	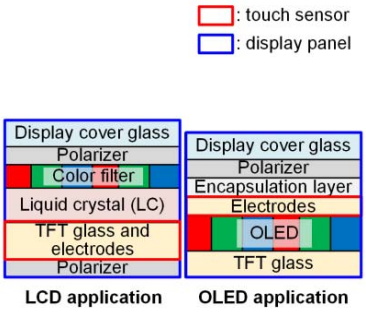
Main applications	- LCD and OLED for large-to-medium sized touch sensors	- OLED for small-to-medium sized mobile touch sensors	- LCD for small-to-medium sized mobile touch sensors

[1] Display devices are the liquid crystal (LC) or organic light emitting diode (OLED) with the thin-film transistor (TFT) glass.

The C_S sensing method achieves high sensitivity, but suffers from accurately detecting the coordinates of the multi-touch fingers because of the ghost points [59], [70]. The *Cs* sensing method is adopted in the AFE IC in an attempt to detect the multi-touch fingers [36], [50]. The touch electrode, which is fabricated by segmenting the common electrodes (V_{COM}s) in the LCD display device, is individually connected with the AFE IC using the trace lines. Since the AFE IC senses the ΔC_Ss of all touch electrodes, it can detect the coordinates of the multi-touch fingers without ghost points. However, the CTSs have a complex manufacturing process due to the trace lines in the display device [36], [50]. Moreover, as the size of the touch sensor increases, the number of touch electrodes increases by the square of the touch sensor size. Therefore, the AFE IC requires a large number of readout circuits, which occupy a large area and increase the manufacturing cost.

B. Mutual-Capacitor (C_M) Sensing Method

Fig. 3(b) shows the C_M sensing method [16], [18], [22]–[23], where the C_M is defined by the capacitance between the TX and RX electrodes in the touch sensor. When the finger touches the touch sensor, it absorbs the electric field, resulting in a decrease in Q_Ss. In the C_M sensing method, the AFE IC sends V_{EXT}s to the TX electrodes and senses the Q_S in the RX electrodes, thus sensing the variation in the C_M (ΔC_M). The C_M sensing method has a lower sensitivity than the C_S sensing method, but can easily detect the multi-touch fingers. Therefore, it can be widely adopted for CTSs. The AFE IC and styli, which adopt the C_M sensing method, will be described in detail in Sections IV and V, respectively.

III. TYPES OF TOUCH SENSORS

As the demand for high performance CTS increases in many applications, more requirements for touch sensors such as high transmittance, and low thickness, light weight, and low manufacturing cost have been demanded. To meet these requirements, several types of touch sensors such as add-on, on-cell, and in-cell types have been researched as listed in Table I.

A. Add-On Type

The add-on type [18], [22], [23], [25], [27]–[28], [30], [31], [34], [35], [38], [44], [45], [47]–[49], [56]–[58] includes the touch sensor (touch cover glass, and TX and RX electrodes) and the liquid crystal display (LCD) display panel (display cover glass, polarizer, color filter, liquid crystal (LC), thin-film transistor (TFT) glass, and polarizer) or organic light emitting diode (OLED) display panel (display cover glass, polarizer, encapsulation layer, OLED, and TFT glass) with an air gap as shown in Table I. The add-on type was first introduced by attaching the 3.5- and 7.0-inch touch sensors on the display panels in 2010 [44], [45]. After that, the touch sensors ranging from 4.3- to 70.0-inches have been used in the CTSs [56]–[58]. The add-on type has been mainly adopted for medium-to-large sized touch applications [56], [57] because of its easy implementation. However, as the touch sensor increases in size, its cut-off frequency (f_{C_TS}) decreases because f_{C_TS} is inversely proportional to the size of the touch sensor. The medium-to-large sized touch sensor, which has a low f_{C_TS}, degrades the SNR. The f_{C_TS} can be increased by using an electrode material with low impedance, resulting in an increase in the SNR.

The indium-tin-oxide (ITO) with high optical transmittance, which is commonly used for fabricating the electrodes of the touch sensor, has a high sheet resistance (150 Ω/□); thus, it is not suitable for the medium-to-large size touch sensors. To enhance the f_{C_TS} of the touch sensor, the metal mesh (silver or copper) [27], [38], [49], [56], [57] or silver nanowire (AgNW) [66], each of which has a low sheet resistance

(silver: 0.2 Ω/□, copper: 0.003 Ω/□, and AgNW: 60 Ω/□), is used for the touch sensor. However, they have visual issues such as moirés or haze [37].

B. On-Cell Type

The on-cell type [29], [46], [51], [59], [60], [69] includes the electrodes of the touch sensor between the polarizer and color filter in the LCD display panel, whereas between the polarizer and encapsulation layer in the OLED display panel, as shown in Table I. The on-cell type was first introduced by integrating the 13.3-inch touch sensor on the color filter in 2011 [51]. After that, the touch sensors ranging from 3.2- to 13.3-inches have been used in the CTSs [46], [51]. The on-cell type was primarily employed for small-to-medium sized mobile touch applications [37] due to its higher transmittance, lower manufacturing cost, less weight, and thinner thickness than the add-on type. However, in the manufacturing process of the display panel, the TX and RX electrodes are deposited on the color filter (LCD display panel) or the encapsulation layer (OLED display panel) in two layers or in a single layer with the bridge metal, and thereby they require an extra fabrication process. In addition, the on-cell type touch sensor is located far from the finger and near to the DDI, thus it is more sensitive to the display noise (V_{DN}), resulting in a lower SNR than the add-on type.

C. In-Cell Type

The in-cell type includes the touch sensor in the LCD or OLED display panels because the touch sensor is integrated in the display devices of the display panel as shown in Table I. The in-cell type was first realized by integrating 4.0-inch touch sensors on the display device in the display panel in 2010 [39]. After that, touch sensors ranging from the 7.0- to 15.6-inches have been used in the CTSs [50]. The in-cell type was employed for the small-to-medium-sized mobile touch applications [36], [50] similarly to the on-cell type. In the manufacturing process of the LCD panel, the electrodes are fabricated by connecting the segmented V_{COM}s through the metal in the TFT glass [36], [50]. However, in the manufacturing process of the OLED panel, the electrodes are fabricated by connecting the segmented cathode electrodes through the metal, but the cathode patterning process can degrade the electrical characteristics of the OLED. Therefore, in-cell type is predominantly adopted in the LCD panels.

Since the touch sensor is integrated with the TFT glass in the display panel, it has less weight, thinner thickness, and lower manufacturing cost than the add-on and on-cell types. The segmented V_{COM}s are used for the electrodes of the touch operation and for the display operation, separately. Therefore, the frame time is divided into touch sensing and display times, and thereby the touch sensing time of the in-cell type can be reduced compared with that of the add-on and on-cell types. In addition, the in-cell type touch sensor is located far from the finger and near to the DDI than the on-cell and add-on types. Therefore, the in-cell type has a lower SNR than the add-on and on-cell types.

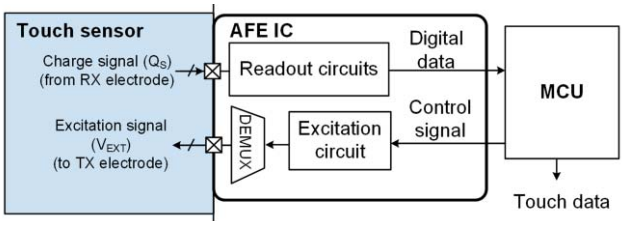

Fig. 4. Block diagram of capacitive touch system (CTS) for the scan driving method (SDM).

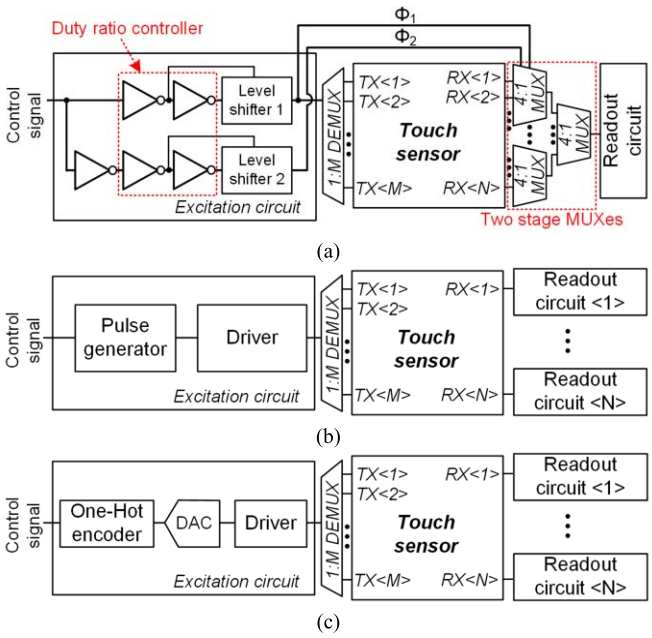

Fig. 5. Structures of the capacitive touch system (CTS) for scan driving methods (SDMs) in (a) [45], (b) [47], and (c) [58].

IV. Analog Front-End (AFE) IC

The AFE ICs are needed to detect the small ΔC_M between the TX and RX electrodes in noisy environments and respond to the fast movement of the finger and styli. To satisfy the above demands, several driving and sensing methods for the AFE ICs have been studied [16], [18], [22], [23], [30], [38], [42]–[45], [47]–[49], [51]–[66], [69]–[71].

A. Driving Methods

1) Scan Driving Method (SDM): Fig. 4 shows the block diagram of the CTS for the SDM. When the excitation circuit receives the control signal from the MCU, it generates the V_{EXT} and sequentially sends it to the TX electrodes through the de-multiplexer (DEMUX). The readout circuit senses the Q_S, which is converted from the V_{EXT}, and extracts the digital data according to the Q_S. The MCU then calculates the touch data using the extracted digital data.

Several CTS structures for the SDM were proposed in [16], [18], [22], [42]–[45], [47], [48], [51], [52], [54], [55], [59]–[61], [64]–[66], and [69]–[71]. The SDM was proposed by Hotelling *et al.* [42], [43] and realized with a CTS as shown in Fig. 5(a) [45]. The CTS includes the one-channel excitation

circuit, 1:M DEMUX, touch sensor, N:1 multiplexer (MUX), and one-channel readout circuit. When the excitation circuit receives the control signal from the MCU, the first stage inverters in the duty ratio controller delay the falling times of the control signal and the inverted control signal. The second stage inverters then generate the non-overlap clock signals (Φ_1 and Φ_2) using the delayed control signal and inverted control signal, respectively. The level shifters 1 and 2 adjust the amplitudes of the Φ_1 and Φ_2, respectively, and transfer them to the first stage 4:1 MUXes. In addition, the adjusted Φ_1 is sent to the touch sensor through the 1:M DEMUX as a V_{EXT}. The touch sensor then converts the V_{EXT} to Q_Ss, which are sequentially selected using the two stage 4:1 MUXes. Since the AFE IC includes the one-channel excitation and readout circuits, it has a simple structure and occupies a small area. However, the delay to control the V_{EXT} in the excitation circuit is easily influenced by the process-voltage-temperature variations. In addition, the sensing time of the one-channel readout circuit is reduced because the frame time (T_{frame}) is shared with the demultiplexing and multiplexing operations at the M-channel TX and N-channel RX electrodes, respectively. Consequently, the SNR of [45], which is proportional to the touch sensing time, is reduced.

The CTS in [47] consists of the one-channel excitation circuit, 1:M DEMUX, touch sensor, and N-channel readout circuits as shown in Fig. 5(b). When the excitation circuit receives the control signal from the MCU, it sends the V_{EXT} to the touch sensor through the pulse generator and driver. The N-channel readout circuits parallelly sense the Q_Ss from the N-channel RX electrodes. Since the AFE IC includes the one-channel excitation and N-channel readout circuits, the touch sensing time of the CTS is N-times higher than that of [45]. In addition, the excitation circuit controls the duty ratio of the V_{EXT} using the pulse generator, and thereby can accurately send the V_{EXT} to the touch sensor. However, the structure of the AFE IC is more complex than that of [45].

The CTS in [58] consists of the one-channel excitation circuit, 1:M DEMUX, touch sensor, and N-channel readout circuits as shown in Fig. 5(c). The excitation circuit includes the one-hot encoder, digital-to-analog converter (DAC), and rail-to-rail buffer as a driver. When the excitation circuit receives the control signal from the MCU, it generates a step-wise triangular waveform using the one-hot encoder and DAC, and sends the V_{EXT} to the touch sensor through the driver. When the readout circuit senses the triangular shaped V_{EXT}, it accurately senses the Q_S because the triangular shaped V_{EXT} has a lower DC offset and higher amplitude of the Q_S than the pulse shaped V_{EXT} [45], [47]. However, the AFE IC has higher complexity and more area than [45], [47] due to the analog blocks (DAC and driver) in the excitation circuit.

2) Parallel Driving Method (PDM): Fig. 6 shows the conceptual diagrams of the SDM and PDM. As shown in Fig. 6(a), the AFE IC sequentially sends the V_{EXT} to all M-channel TX electrodes and divides its T_{frame} by the number of TX electrodes. Thus, the touch sensing time of each TX electrode for SDM ($T_{SEN,SDM}$) is determined to be T_{frame}/M, where M is the number of TX electrodes. Therefore, the SNR

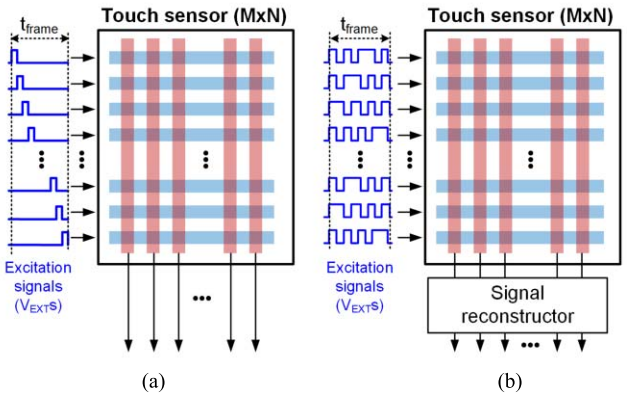

Fig. 6. Conceptual diagrams of (a) scan driving method (SDM) and (b) parallel driving method (PDM).

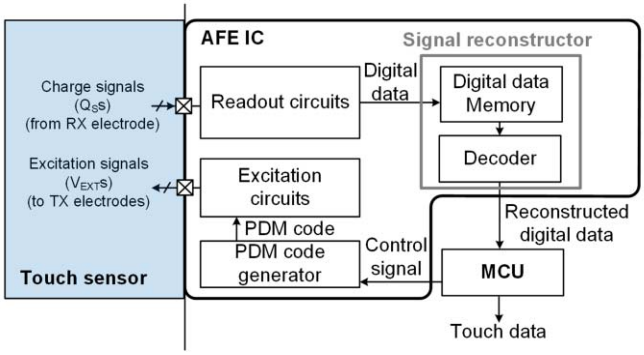

Fig. 7. Block diagram of the capacitive touch system (CTS) for the parallel driving method (PDM) [53].

of the AFE IC decreases as $T_{SEN,SDM}$ decreases because the number of averaging operations required to sense the Q_S proportionally decreases with $T_{SEN,SDM}$ [38]. To enhance the SNR while maintaining a short $T_{SEN,SDM}$, the AFE IC should generate high V_{EXT}, but needs high voltage devices, resulting in an increase in chip area and manufacturing cost [56]. As shown in Fig. 6(b), the AFE IC parallelly sends the V_{EXT}s with orthogonal matrices to all M-channel TX electrodes and determines its touch sensing time of each TX electrode for PDM ($T_{SEN,PDM}$) to be T_{frame}. Since the $T_{SEN,PDM}$ is M-times longer than $T_{SEN,SDM}$, the amplitude of Q_S of the PDM becomes M-times higher than that of the SDM. In addition, the induced external noise of the PDM is $\sqrt{M}$ times higher than that of the SDM. Therefore, the SNR of the PDM is improved by $\sqrt{M}$-times higher than that of the SDM [38], [56].

The first CTS for the PDM was proposed as shown in Fig. 7 [49]. In the CTS, the AFE IC consists of the readout and excitation circuits, PDM code generator, and signal reconstructor with digital data memory and a decoder. The PDM code generator generates the PDM code and sends it to the excitation circuits according to the control signal transferred from the MCU. The excitation circuits send the orthogonal matrices, such as a Walsh-Hadamard sequence [53] and Maximum-length sequence [56], [57], to the TX electrodes. The readout circuits parallelly receive the Q_S from all

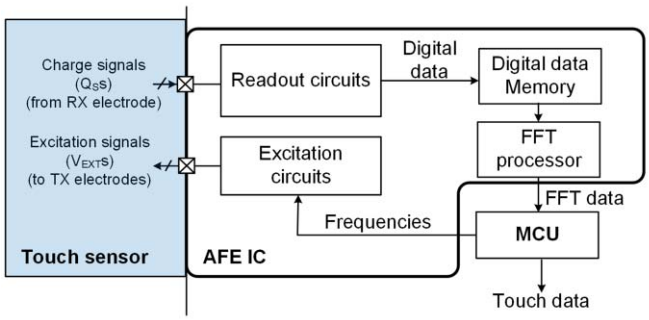

Fig. 8. Block diagram of the capacitive touch system (CTS) for the multiple frequency driving method (MFDM) [49], [91], [93].

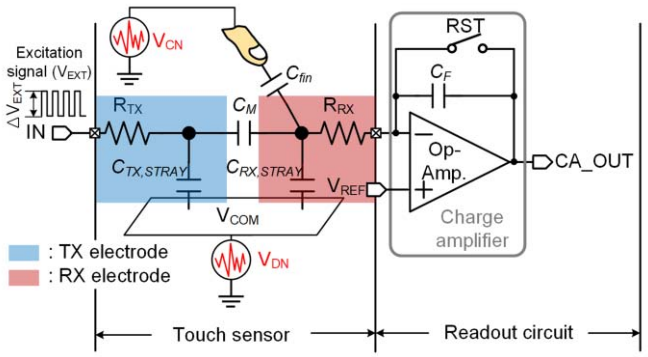

Fig. 9. Block diagram of the touch sensor and readout circuit using single channel sensing method.

TABLE II
COMPARATIVE ANALYSIS OF THE DRIVING METHODS

Types	Scan driving method (SDM) [16], [18], [22], [42]–[45], [47], [48], [51], [52], [54], [55], [59]–[61], [64]–[66], [69]–[71]	Parallel driving method (PDM) [23], [30], [38], [53], [56]–[57], [62]–[63]	Multiple frequency driving method (MFDM) [49], [91], [93]
Pros	- Simple structure - Small area	- High SNR (long sensing time)	- High SNR (long sensing time) - High frame rate
Cons	- Low SNR (short sensing time) - Large chip area and manufacturing cost due to the high voltage devices	- High power consumption - Low frame rate at the large number of TX electrodes - Large area and high complexity due to the signal reconstructor	- High power consumption - Large area and high complexity due to the FFT processor

RX electrodes and convert it to the digital data. The signal reconstructor receives the digital data from the readout circuits, and stores it into the digital data memory. After the Q_Ss are sensed by the readout circuit for T_{frame}, the decoder converts the digital data to the reconstructed digital data. The MCU receives the reconstructed digital data and extracts the touch data. Thus, the PDM can achieve a high SNR without using high voltage devices, but has high power consumption because the M-channel excitation circuits simultaneously send the V_{EXT}s to all TX electrodes. In addition, the AFE IC requires a large area and high complexity due to the signal reconstructor.

3) Multiple Frequency Driving Method (MFDM): Although the PDM achieves a higher SNR compared to the SDM, the size of the orthogonal matrices increases as the number of TX electrodes increases, thus increasing T_{frame}. To achieve the high frame rate regardless of the size of the touch sensor (the number of TX electrodes), the MFDM was first introduced in [49], [91], and [93]. As shown in Fig. 8, the AFE IC for the MFDM consists of the readout and excitation circuits, digital data memory, and fast Fourier transform (FFT) processor. The MCU firstly detects the external noises using an FFT processor without emitting the V_{EXT}. The MCU locates the frequencies of V_{EXT}s in the low-noise regions. The excitation circuits send the V_{EXT}s, of which all the different frequencies are transferred from the MCU, to all the TX electrodes. The readout circuits receive the induced Q_S from the RX electrodes and convert it to the digital data. The digital memory stores the digital data and transfers it to the FFT processor. The FFT processor converts the digital data (time domain) to the FFT data (frequency domain) because each V_{EXT} has a different frequency. The MCU then extracts the touch data using the FFT data. Since the MCU locates the frequencies of V_{EXT}s in the low-noise region, the AFE IC are not influenced from the external noises. In addition, the T_{frame} of the AFE IC for MFDM ($T_{frame,MFDM}$) is determined to be $(N_{DFFT} \times N_{READ,ADC})/(f_{CONV,ADC})$, where N_{DFFT}, $f_{CONV,ADC}$, and $N_{READ,ADC}$ are the number of time-divided digital data, which is transferred into the FFT processor, the conversion frequency of the ADC, and the number of readout circuits per ADC, respectively. The frame rate of the MFDM can be higher than that of the SDM and PDM because the MFDM is not correlated with the number of TX electrodes. However, the AFE IC has high power consumption because the M-channel excitation circuits simultaneously send the V_{EXT}s to the touch sensor. In addition, the FFT processor in the AFE IC occupies a large area and has a higher complexity. The comparative analysis of the driving methods is listed in Table II.

B. Sensing Methods of Analog Front-End (AFE) IC

Fig. 9 shows the block diagram of the touch sensor and readout circuit using a single channel sensing method. The touch sensor is modeled with the resistances of the TX and RX electrodes (R_{RX} and R_{TX}), and the capacitance between V_{COM} and two electrodes ($C_{TX,STRAY}$ for the TX electrode and $C_{RX,STRAY}$ for the RX electrode). The charge amplifier consists of the operational amplifier (Op-Amp.), reset switch (RST), and feedback capacitor (C_F) [71]. Its output signal (V_{CA_OUT}) for a step of the V_{EXT} is defined as $V_{REF} - V_{EXT} \times (C_M/C_F)$, where V_{REF} is a reference voltage to bias the charge amplifier. The external noises, such as conduction and display noises (V_{CN} and V_{DN}), are also induced into the readout circuit [51]–[71]. The V_{CN} and V_{DN} are coupled with the finger capacitor (C_{fin}), and $C_{RX,STRAY}$ and $C_{TX,STRAY}$, respectively. Since the external noises (V_{CN} and V_{DN}) are continuously induced into the readout circuit, V_{CA_OUT} can

TABLE III
DETAILED EQUATIONS OF V_{CA_NOISE}

V_{CA_NOISE}	Equations
$\lvert V_{CN}\rvert$	$\frac{C_{fin}}{C_F}\times V_{CN}$
$\lvert V_{DN}\rvert$	$\frac{\left(C_{RX,STRAY}+\frac{C_{TX,STRAY}\times C_M}{C_{TX,STRAY}+C_M}\right)}{C_F}\times V_{DN}$

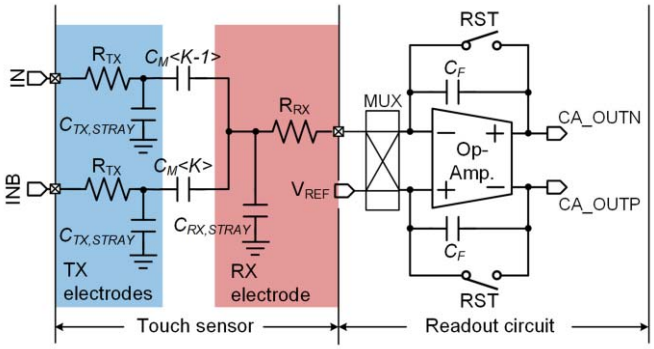

Fig. 10. Block diagram of the touch sensor and readout circuit using differential sensing method [51].

be modified to be

$$V_{CA\_OUT} = V_{EXT} - \frac{C_M}{C_F} \times V_{EXT} + V_{CA\_NOISE}, \quad (1)$$

where V_{CA_NOISE} is the output voltage of the charge amplifier due to V_{CN} and V_{DN} that degrade the SNR of the AFE IC. The detailed equations of the V_{CA_NOISE} are expressed in Table III. To enhance the SNR, several differential and chopper stabilization sensing methods have been researched [51]–[71].

1) Differential Sensing Method: To enhance the SNR, the CTS with differential sensing method was first introduced in [51]. The proposed readout circuit includes the fully differential Op-Amp. and multiplexer (MUX) as shown in Fig. 10. When the complementary V_{EXT}s are sent to the two adjacent TX electrodes, the two Q_Ss, which are in a reciprocal phase, are superposed at the RX electrode. Therefore, when the external noises (V_{CN} and V_{DN}) are continuously induced into the readout circuit, the output voltages at the output nodes (CA_OUTP and CA_OUTN) are derived as

$$V_{CA\_OUTP} = V_{REF} - \frac{C_M\langle K-1\rangle - C_M\langle K\rangle}{C_F} \times V_{EXT} + V_{CA\_NOISE}, \quad (2)$$

and

$$V_{CA\_OUTN} = V_{REF} - \frac{C_M\langle K\rangle - C_M\langle K-1\rangle}{C_F} \times V_{EXT} + V_{CA\_NOISE}, \quad (3)$$

where $C_M < K-1 >$ and $C_M <$ K $>$ are C_Ms at the (K-1)th and Kth TX electrodes, respectively. Since the fully differential Op-Amp. derives the difference between V_{CA_OUTP} and V_{CA_OUTN}, the differential output voltage (V_{CA_OUT}) is determined to be

$$V_{CA\_OUT} = -2 \times \frac{C_M\langle K-1\rangle - C_M\langle K\rangle}{C_F} \times V_{EXT}. \quad (4)$$

When the finger touches the (K-1)th TX electrode, the value of $C_M < K-1 >$ is only reduced, and thereby the variation in C_M is only sensed in the readout circuit that can enlarge the dynamic range of V_{CA_OUT} with filtering the external noises. Various AFE ICs have adopted the differential sensing method to filter out external noises using various sizes of the touch sensors [51]–[66]. However, when the amplitudes of external noises at the two adjacent RX electrodes are different, the AFE IC cannot effectively attenuate the external noises.

2) Chopper Stabilization Sensing Method: The chopper stabilization sensing methods have been used to achieve a high SNR in various AFE ICs using a single RX electrode [67]–[71]. The chopper stabilization sensing method was first introduced in [67]. Fig. 11(a) and (b) show the block diagram of the touch sensor and readout circuit using a chopper stabilization sensing method, and the frequency spectral in the readout circuit, respectively. The readout circuit consists of the charge amplifier, anti-harmonic filter, demodulator, and LPF. When the V_{EXT}, which has the frequencies of f_{EXT} and its harmonics (f_{EXT_H}), is sent to the touch sensor, the V_{EXT} and external noises (V_{CN} and V_{DN}) are superposed. The readout circuit senses the Q_S and attenuates the external noises because the touch sensor and charge amplifier operate as the 1st order LPF and high-pass filter, respectively. The anti-harmonic filter, which operates as an LPF, filters out the harmonics of the V_{EXT}. The demodulator demodulates the output voltage of the anti-harmonic filter (V_{AHF}) to the DC signal and modulates the external noises to the high-frequency spectrum. The LPF filters out only the modulated external noises.

The chopper stabilization sensing method achieves a high SNR by separating the f_{EXT} and frequency of the external noise and filtering out the external noises. However, it senses the total value of C_M, and thereby the dynamic range of the AFE IC using the chopper stabilization sensing method is narrower than that using the differential sensing method. In addition, when the f_{EXT} is located near the frequency of external noises, the external noises are not filtered out. To overcome the above issue, the adaptive chopper stabilization sensing method was introduced in [71]. The adaptive chopping controller calculates the amplitude of external noises, which are induced into the AFE IC, and selects an optimal set of operational frequencies of band-pass filter, demodulator, and LPF, and thereby the CTS achieved high noise immunity. However, it requires a complex structure because the band-pass filter, demodulator, and LPF are synchronously controlled according to the frequency of the V_{EXT}. Table IV shows the comparative analysis of the sensing methods.

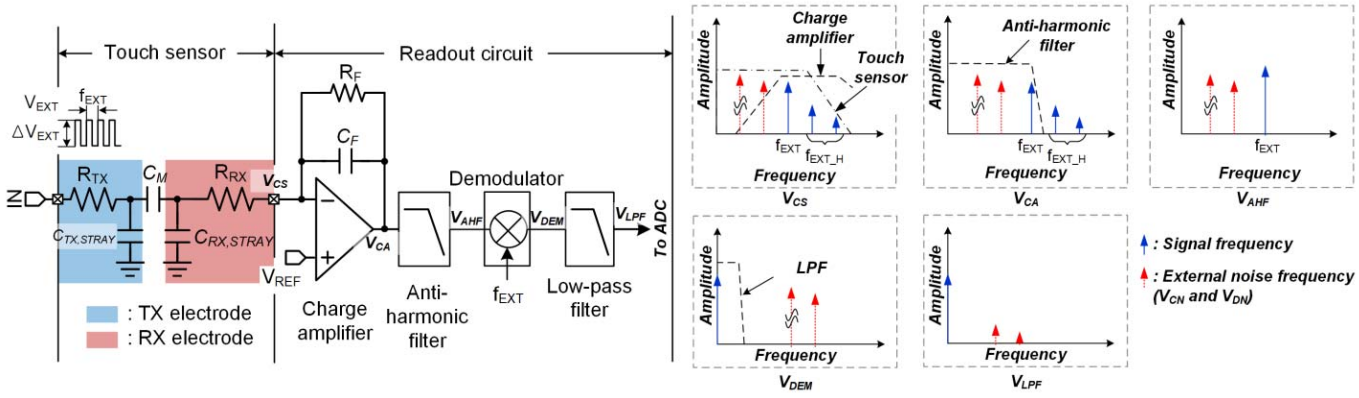

Fig. 11. (a) Block diagram of touch sensor and readout circuit using the chopper stabilization sensing method, and (b) the frequency spectral in the readout circuit [67].

TABLE IV
COMPARATIVE ANALYSIS OF SENSING METHODS

Types	Differential sensing method [51]–[66]	Chopper stabilization sensing method [67]–[71]
Pros	- Simple structure - Wide dynamic range	- High SNR
Cons	- Low SNR when the amplitudes of external noises at two adjacent RX electrodes are different.	- Complex structure - Narrow dynamic range - Low SNR when f_{EXT} is located near the frequency of external noises

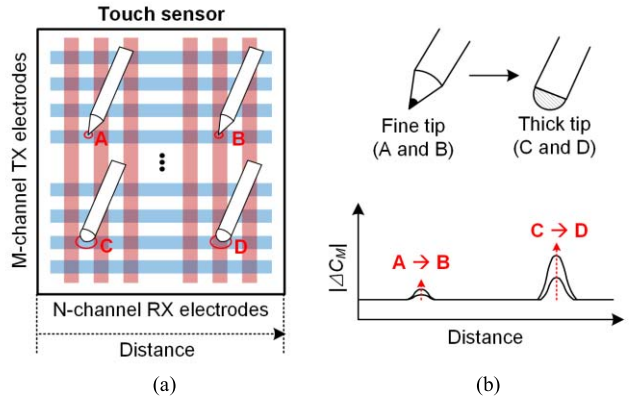

Fig. 12. Conceptual diagram of capacitive type passive stylus: (a) touch position of the stylus and (b) capacitance profiles according to the touch positions and stylus tip thickness [72].

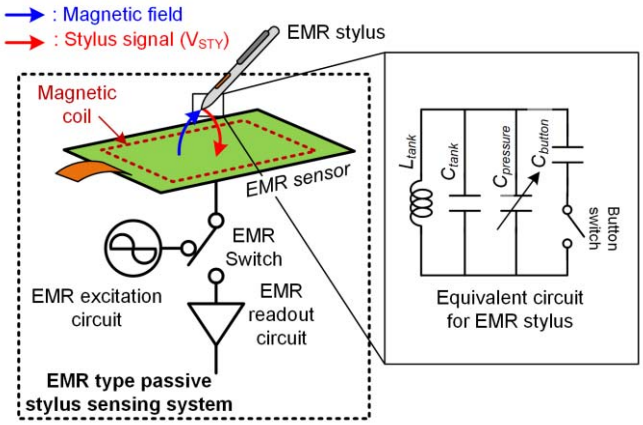

Fig. 13. Conceptual diagram of an electromagnetic resonance (EMR) type passive stylus and sensing system [73]–[76].

V. STYLUS TECHNOLOGIES

A. Passive Stylus

1) Capacitive: The capacitive type passive stylus, which is a conceptual extension of the hand and as such will practically work with any CTS, has been widely used in the CTS because of its light weight and low cost [72]. Fig. 12 shows the conceptual diagram of the capacitive type passive stylus. When the touch position of the stylus moves from point A or C (between two RX electrodes) to point B or D (on the RX electrode), respectively, the absolute ΔC_M ($|\Delta C_M|$) increases because the stylus absorbs more Q_S. Also, as the stylus tip increases in size, it absorbs more Q_S between the tip and electrodes, resulting in an increase in $|\Delta C_M|$. Thus, the capacitive type passive stylus depends on the size of the tip and electrode pitch. As the stylus tip decreases in size, it absorbs less electric field from the electrodes, resulting in a decrease in ΔC_M, and thereby it is hard to detect the stylus coordinate [72]. Therefore, a thick tip is used for the capacitive type passive stylus so as to absorb the more electric field, resulting in an increase in ΔC_M. To detect the stylus coordinate when the styli with a fine tip is used, the styli manufacturers used to attach the see through disc at the tip so that the more electric field can be absorbed. A capacitive type passive stylus is easy to use because it is thin and light. However, it has low SNR, low accuracy, and limited drawing expressions. Especially, the regular pencil can be utilized as a passive stylus in the CTS with the eraser feature [25], but this has not been commercialized yet.

2) Electromagnetic Resonance (EMR): The EMR type passive stylus, on which it is easy to implement additional functions, has been adopted for mobile phones [73]–[76]. Fig. 13 shows the conceptual diagram of the EMR type passive

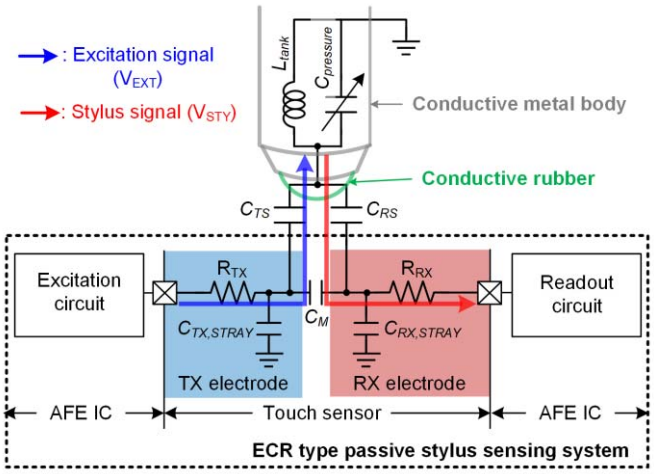

Fig. 14. Conceptual diagram of an electrically coupled resonance (ECR) type passive stylus and sensing system [77]–[79].

stylus and sensing system including the EMR sensor with magnetic coils, EMR switch, and EMR excitation and readout circuits. The EMR type passive stylus is composed of the tank inductor (L_{tank}), tank capacitor (C_{tank}), and pressure-sensitive capacitor ($C_{pressure}$), button capacitor (C_{botton}), and button switch. It absorbs the magnetic field through the L_{tank} and combination of capacitors ($C_{tank}+C_{pressure}+C_{botton}$), which is generated from the magnetic coils in the EMR sensor. It then converts the absorbed magnetic field to a radio frequency (RF) signal and transmits the RF signal back to the EMR sensor as a stylus signal (V_{STY}) [73]–[76]. When the readout circuit is connected to the EMR sensor through the EMR switch, it senses the transmitted V_{STY}. Thus, the pressure of the EMR type passive stylus can be expressed using a different frequency of the V_{STY}, which is determined by the L_{tank} and $C_{tank}+C_{pressure}+C_{botton}$, by changing the value of $C_{pressure}$. The EMR type passive stylus uses the LC-resonator, where the L is inductively coupled to the magnetic coils in the EMR sensor as described in Section V.A.2). On the other hand, the ECR type passive stylus receives the resonance signal from the V_{EXT} and sends it to the TSP. The AFE IC in the CTS then senses the resonance signal through the capacitive coupling with the TSP. Although the EMR type stylus can express the pressure and tilt angle with a narrow tip, it needs the additional EMR sensor to generate and sense the RF signal, and thereby the power consumption and manufacturing cost increase, and the CTS becomes thicker up to 600 μm [37]. In addition, since the accuracy of the EMR stylus depends on the number of magnetic coils in the EMR sensor, it is necessary to evenly place the EMR sensor underneath the touch sensor.

3) Electrically Coupled Resonance (ECR): The ECR type passive stylus was proposed in an attempt to express the pressure without an additional magnetic sensor [77]–[79]. Fig. 14 shows the conceptual diagram of the ECR type passive stylus and sensing system including the touch sensor and AFE IC. The ECR type passive stylus consists of the conductive rubber and metal body including L_{tank} and $C_{pressure}$. It absorbs the V_{EXT} through the capacitor between the stylus and the TX electrode of the touch sensor (C_{TS}), which is sent from the excitation circuit in the AFE IC. It then converts the absorbed V_{EXT} to the resonance signal and transmits the resonance signal to the touch sensor as a V_{STY} with a frequency of $1/(2\pi\times\sqrt{(L_{tank}\times C_{pressure})})$. The readout circuit senses the V_{STY} through the capacitor between the stylus and the RX electrode of the touch sensor (C_{RS}). Thus, the pressure of the ECR type passive stylus can be expressed using a different frequency of V_{STY}, which is determined by the L_{tank} and $C_{pressure}$, by changing the value of $C_{pressure}$. The ECR type passive stylus does not need an additional magnetic sensor in the CTS, thus achieving low power consumption, low manufacturing cost, and thin CTS, but there still remains a problem in pressure accuracy. In addition, it cannot easily absorb the V_{EXT} through the C_{TS} because the C_{TS} has a small capacitance value, thus achieving a low SNR. Therefore, to enhance the SNR, the CTS should have a high voltage of V_{EXT}, which requires high-voltage devices, thus increasing the chip area and manufacturing cost.

B. Active Stylus

The active stylus was first adopted in the CTS with the PDM in an attempt to express the pressure and hovering height with high SNR [84]. To realize the PDM in a number of active styli and AFE ICs, the active styli need to send the orthogonal matrices in accordance with the excitation circuits, thus requiring the synchronization with the AFE IC as shown in Fig. 15(a). The active stylus absorbs the synchronization signals, which are generated from the AFE IC, to synchronize with the AFE IC. To extract the coordinates of the active stylus, the AFE IC separately senses the V_{STY} from the RX and TX electrodes [80]–[94] by inserting the synchronized phase before the RX and TX coordinate sensing phases, respectively. Fig. 15(b) shows the RX coordinate sensing phase. After the first synchronization phase, the two active styli (stylus 1 and stylus 2) and AFE IC send the two V_{STY}s (V_{STY1} and V_{STY2}), and M-V_{EXT}s, respectively, to the touch sensor. The AFE IC senses the V_{STY1}, V_{STY2}, and M-V_{EXT}s, and reconstructs the N×(M+2) matrix digital data through the signal reconstructor, thus extracting the RX coordinates of the active styli. Fig. 15(c) shows the TX coordinate sensing phase. The TX coordinates of the active styli are extracted by driving the excitation circuit and sensing the readout circuit in the opposite directions to those in Fig. 15(b). After the second synchronization phase, the styli 1 and 2, and AFE IC send V_{STY1}, V_{STY2}, and N-V_{EXT}s, respectively, to the touch sensor. The AFE IC reconstructs the (N+2)×M matrix digital data through the signal reconstructor, thus extracting the TX coordinates of the active styli. In the RX and TX coordinate sensing phases, the AFE IC extracts the two-dimensional coordinates of the active styli. The active stylus is synchronized with the AFE IC using one or two pulse signals [94], the frame rate required to sense the active styli is almost half of that for sensing a finger. Although the active stylus can express the pressure and hover height with high SNRs, the additional sensing circuitry is needed in the active stylus for sensing the synchronization signals.

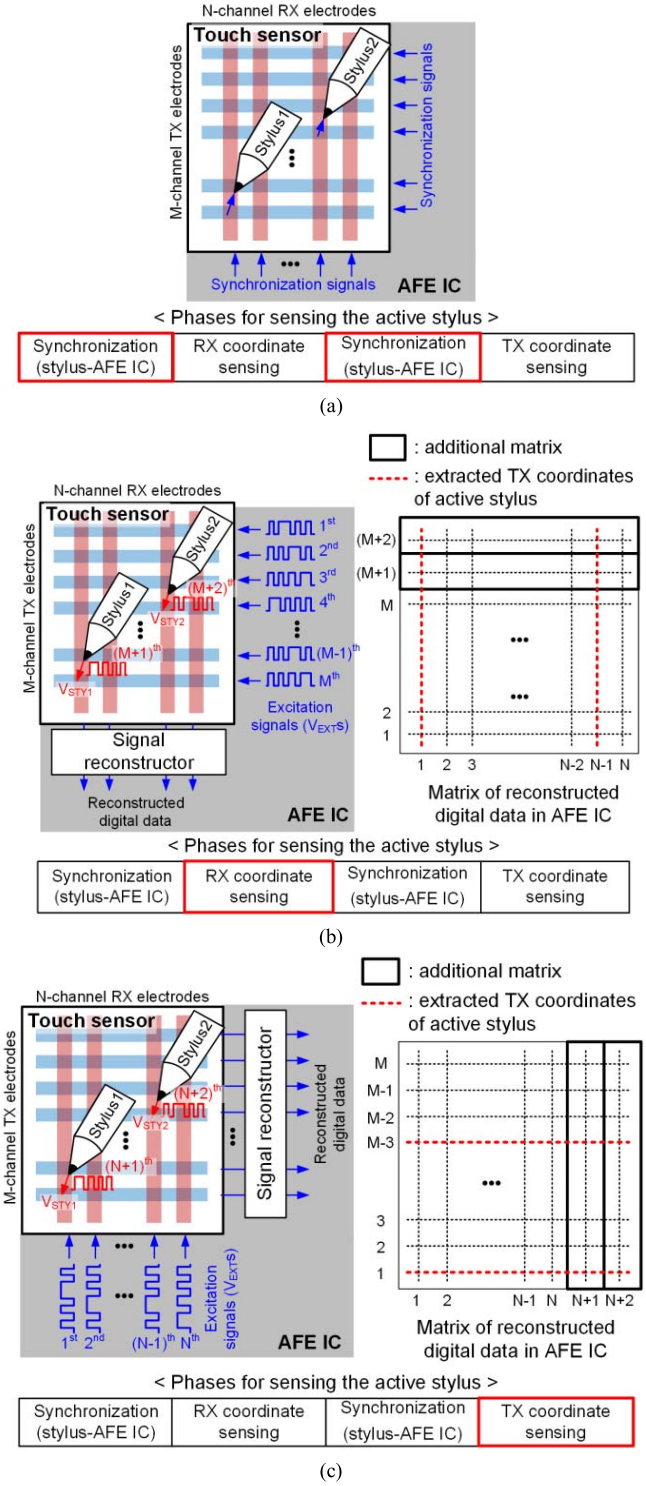

Fig. 15. Conceptual diagram of active stylus and sensing system [90], [94]: (a) synchronization phases, (b) RX coordinate sensing phase and (c) TX coordinate sensing phase.

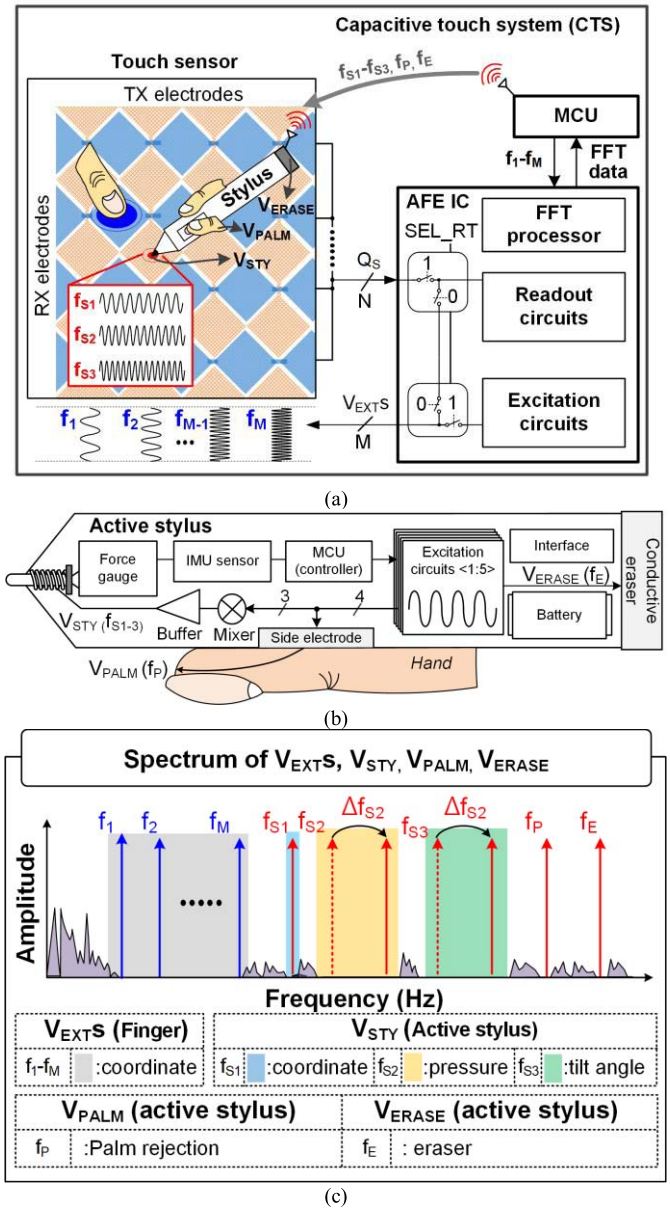

Fig. 16. Conceptual diagram of the capacitive touch system (CTS) and active stylus using the multiple frequency driving method (MFDM) [49], [91], [93]: (a) CTS, (b) active stylus, and (c) operational principle.

The active stylus is adopted in the CTS with MFDM [49], [91], [93] in an attempt to remove the additional synchronization phases and enrich the expression with high SNR. The Fig. 16(a), (b), and (c) show the conceptual diagrams of the CTS and active stylus, and operational principle, respectively. As shown in Fig. 16(a), the wire or wireless communication between the MCU and active stylus is operated by transferring only the frequency information (f_{S1}: coordinate of active stylus, f_{S2}: pressure, f_{S3}: tilt angle, f_P: palm rejection, and f_E: eraser) to the active stylus without timing synchronization [49], [91], [93]. The active stylus then sends the V_{STY}, V_{PALM}, and V_{ERASE}, which contains the f_{S1}-f_{S3}, f_P, and f_E, respectively, to the touch sensor. As shown in Fig. 16(b), the active stylus includes the force gauge, inertial measurement unit (IMU), signal controller, five excitation circuits, mixer, buffer, wireless IC, battery, side electrode, and conductive eraser. Firstly, when the pressure and tilt angle are sensed by the IMU and gyro sensor, the signal controller transfers the Δf_{S2} and Δf_{S3} to the excitation circuits, respectively. The excitation circuits generate five V_{EXT}s with frequencies of f_{S1}-f_{S3}, f_P, and f_E.

TABLE V
COMPARATIVE ANALYSIS OF STYLUS TECHNOLOGIES

Types	Pros	Cons
Capacitive type passive stylus [72]	- Thin and light - Low cost	- Limited drawing expressions - Low SNR and accuracy
Electromagnetic resonance (EMR) type passive stylus [73]–[76]	- Express the pressure and tilt angle with narrow tip	- Additional EMR sensor needs the power consumption, manufacturing cost, and CTS becomes thicker - Accuracy of stylus depends on the number of magnetic coils in the EMR sensor
Electrically coupled resonance (ECR) type passive stylus [77]–[79]	- Does not need an additional sensor - Low power consumption - Low manufacturing cost - Thin CTS	- Low pressure accuracy - Low SNR
Capacitive type active stylus [80]–[94]	- Various drawing expressions such as pressure, hover height, tilt angle, palm rejection, and eraser - High SNR	- Thickness, power consumption, and manufacturing cost increase due to the additional circuit and battery in the active stylus

TABLE VI
FUTURE PERSPECTIVES IN THE CAPACITIVE TOUCH SYSTEM (CTS) AND STYLI

Lists	Small-to-medium sized touch sensor	Medium-to-large sized touch sensor
Touch sensors [27], [38], [49], [56]–[57], [66]	- Low impedance - Visual issues such as moirés and haze - Low manufacturing cost - High sensitivity, linearity, and accuracy	
AFE IC [51]–[71], [95]–[119]	- High frame rate - High SNR - Small die area - Low-power consumption	
	- Integrate the various sensing ICs and DDIs	-
Styli [72]–[94]	- Various drawing expressions with high resolutions (pressure, tilt angle, hover height) - Palm rejection technique without heavy computational load - Low manufacturing cost - Thin thickness and light weight	
Variable applications [93], [119]–[130]	- Digital stationary - Tele-conference or electrical or white board with real-time communication - Haptic interface	

The mixer combines three V_{EXT}s having f_{S1}-f_{S3}, and the buffer then transfers the combined V_{EXT} to the touch sensor as a V_{STY}. At the same time, the excitation circuit sends the V_{PALM} with f_P to the touch sensor as a V_{PALM} through the side electrode and human body. In addition, the excitation circuit generates a V_{EXT} having f_E to the touch sensor as a V_{ERASE} via the conductive eraser to perform the erase operation. As shown in Fig. 16(c), when the AFE IC senses the adjusted frequencies (Δf_{S2} and Δf_{S3}), the MCU can detect the pressure and tilt angle without synchronization. In addition, when the AFE IC senses the frequencies f_P and f_E, the MCU identifies the presence of palm and eraser, respectively. The MCU then detects a capacitance profile of f_P corresponding to V_{PALM} and removes it. In the same way, the MCU detects a capacitance profile of f_E corresponding to V_{ERASE} and erases the displayed touch coordinates. The proposed active stylus achieves various expressions such as the pressure, tilt angle, palm rejection, and eraser. In addition, the active stylus does not degrade the frame rate due to no synchronization phases. Although the active stylus can express the pressure, hovering height, and tilt angle with a high SNR, its thickness, power consumption, and manufacturing cost increase due to the additional circuit and battery in the active stylus. Table V shows the comparative analysis of the stylus technologies.

VI. FUTURE PERSPECTIVES

As previously described, the CTSs and styli have been widely used in various applications, but there remain many requirements to improve the performance of the touch sensor, AFE IC, and styli as listed in Table VI.

A. Touch Sensor

As discussed in Section III, as the touch sensor is enlarged, it needs to use a lower impedance materials such as metal mesh (silver or copper) [27], [38], [49], [56], [57] or AgNW [66]. However, since the low impedances materials are not sufficiently transparent, they should overcome visual issues such as moirés and haze [37]. In addition, the touch sensor needs to minimize the manufacturing cost by reducing the number of electrodes, but its sensitivity is degraded due to its wide electrode pitch. Therefore, a touch sensor with a high sensitivity, linearity, and accuracy should be researched to achieve the high-performance CTS.

B. Analog Front-End (AFE) IC

As discussed in Section IV, the AFE IC with the driving and sensing methods has been reported to have a high frame rate and SNR [51]–[71]. The high frame rate and SNR of the AFE IC enhance the responsiveness to the fast movement of a finger or styli, and sensitivity of the small variation in C_S or C_M, respectively. Moreover, there still remain various researches for AFE IC to achieve the small die area and low-power consumption while maintaining the high frame rate and SNR. Until recently, the AFE ICs for the CTS and DDIs have been integrated into the mobile devices to reduce the manufacturing costs [113]–[115]. To further reduce the manufacturing cost, the AFE IC for CTS should be integrated with DDIs and various sensor ICs such as CMOS image sensors [95]–[98], fingerprint sensors [99]–[112], and force touch sensors [116]–[118].

C. Active and Passive Styli

As discussed in Section V, the styli need to have various expressions with a high resolution, low manufacturing cost, thin thickness, and light weight. Moreover, various expressions such as pressure, tilt angle, and hovering height, the palm rejection technology with low computational load are necessary for the CTS and styli [72]–[94]. When the passive and

active styli are used, the user's palm inevitably touches the touch sensor. To distinguish between the coordinates of the styli and palm, the CTSs need the palm rejection algorithms, which require a lot of computational load [92]. Therefore, the palm rejection technique should be intensively researched for the CTS and styli to reduce the heavy computational load [93]. Moreover, for thin and light styli with low cost, studies to realize the passive styli, which have no additional sensors with various expressions with high resolution, need to be carried out. In addition, the active stylus should be fabricated using a small-sized circuit to reduce its thickness and weight.

D. Various Applications

The CTSs should be adopted in the various applications more extensively [119]–[130]. To realize this, the stationaries, such as notebooks, pencils, erasers, and whiteboards, should be converted from the analog domain to the digital domain because the digital stationaries can share the written data or figures rapidly and easily among various users via the cloud service [130]. In addition, the CTSs, which use the large-sized touch sensors, should be adopted for the tele-conferences or electrical white boards. Thus, during the meeting, the presentation image and/or the coordinates of touch or styli can be rapidly shared with members and stored on a real-time basis [93], [126]–[130]. Moreover, with the use of real-time communications for the presentation image and coordinates of finger and styli, the limitations in time and distance can be overcome. Lastly, the CTSs need to be converged into a haptic interface to provide a reality experience from the electronics to the user [119]–[125].

VII. Conclusion

This paper presents the latest progress in development and applications of the CTSs with styli: touch sensors, AFE IC, passive and active styli. (1) The touch sensors are classified into the add-on, on-cell, and in-cell types according to the size and display devices (LCD or OLED). (2) The driving and sensing methods of the AFE IC are explained in achieving the high SNR and frame rate of the AFE IC. (3) The stylus technologies for CTS were presented with operational principles, advantages, and disadvantages. (4) Future perspectives are given from the viewpoint of technical developments. The CTSs have been widely researched for tens of years, but there still remain many issues in enhancing the performances of CTSs and diversifying the applications. Therefore, the further researches for the touch sensor, AFE IC, passive and active styli are still very important for the CTSs and styli.

References

[1] R. Adler and P. J. Desmares, "An economical touch panel using SAW absorption," *IEEE Trans. Ultrason., Ferroelect., Freq. Control*, vol. UFFC-34, no. 2, pp. 195–201, Mar. 1987.

[2] D. Marioli, E. Sardini, and A. Taroni, "Ultrasonic distance measurement for linear and angular position control," *IEEE Trans. Instrum. Meas.*, vol. IM-37, no. 4, pp. 578–581, Dec. 1988.

[3] H. Nonaka and T. Da-te, "Ultrasonic position measurement and its applications to human interface," *IEEE Trans. Instrum. Meas.*, vol. 44, no. 3, pp. 771–774, Jun. 1995.

[4] D. Marioli, C. Narduzzi, C. Offelli, D. Petri, E. Sardini, and A. Taroni, "Digital time-of-flight measurement for ultrasonic sensors," *IEEE Trans. Instrum. Meas.*, vol. 41, no. 1, pp. 93–97, Feb. 1992.

[5] A. M. Sabatini, "A digital signal-processing technique for compensating ultrasonic sensors," *IEEE Trans. Instrum. Meas.*, vol. 44, no. 4, pp. 869–874, Aug. 1995.

[6] Y. Liu, J. P. Nikolovski, N. Mechbal, M. Hafez, and M. Vergé, "An acoustic multi-touch sensing method using amplitude disturbed ultrasonic wave diffraction patterns," *Sens. Actuators A, Phys.*, vol. 162, no. 2, pp. 394–399, 2010.

[7] Y. Yang, B. Lemaire-Semail, F. Giraud, M. Amberg, Y. Zhang, and C. Giraud-Audine, "Power analysis for the design of a large area ultrasonic tactile touch panel," *Eur. Phys. J. Appl. Phys.*, vol. 72, no. 1, 2015, Art. no. 11101.

[8] Y. Lee *et al.*, "A α-Si:H thin-film phototransistor for a near-infrared touch sensor," *IEEE Electron Device Lett.*, vol. 36, no. 1, pp. 41–43, Jan. 2015.

[9] J. Y. Han, "Low-cost multi-touch sensing through frustrated total internal reflection," in *Proc. 18th Annu. ACM Symp. User Interface Softw. Technol.*, 2005, pp. 115–118.

[10] C.-T. Chuang, T. Chang, P.-H. Jau, and F.-R. Chang, "Touchless positioning system using infrared LED sensors," in *Proc. IEEE Int. Conf. Syst. Sci. Eng. (ICSSE)*, Shanghai, China, Jul. 2014, pp. 261–266.

[11] S. H. Bae *et al.*, "Integrating multi-touch function with a large-sized LCD," in *Soc. Inf. Display (SID) Symp. Dig.*, 2008, pp. 178–181.

[12] E. So, H. Zhang, and Y.-S. Guan, "Sensing contact with analog resistive technology," in *Proc. IEEE Int. Conf. Syst., Man (SMC)*, vol.2. Tokyo, Japan, Oct. 1999, pp. 806–811.

[13] R. N. Aguilar and G. C. M. Meijer, "Fast interface electronics for a resistive touch-screen," in *Proc. IEEE Sensors*, vol. 2, Jun. 2002, pp. 1360–1363.

[14] W.-Y. Chang and H.-J. Lin, "Real multitouch panel without ghost points based on resistive patterning," *J. Display Technol.*, vol. 7, no. 11, pp. 601–606, Nov. 2011.

[15] A. Damilano, H. M. A. Hayat, A. Bonanno, D. Demarchi, and M. Crepaldi, "A flexible low-power 130 nm CMOS read-out circuit with tunable sensitivity for commercial robotic resistive pressure sensors," *IEEE Sensors J.*, vol. 15, no. 11, pp. 6650–6658, Nov. 2015.

[16] Y.-S. Jang, K.-U. Gwak, S.-S. Lee, S.-G. Lee, J.-H. Kim, and H.-S. Oh, "A charge-share-based relative read-out circuit for capacitance sensing," in *Soc. Inf. Display(SID) Symp. Dig.*, 2010, pp. 1937–1939.

[17] C. Luo, M. A. Borkar, A. J. Redfern, and J. H. McClellan, "Compressive sensing for sparse touch detection on capacitive touch screens," *IEEE J. Emerg. Sel. Topics Circuits Syst.*, vol. 2, no. 3, pp. 639–648, Sep. 2012.

[18] B. Liu, Z. Hoseini, K. S. Lee, and Y. M. Lee, "On-Chip touch sensor readout circuit using passive sigma-delta modulator capacitance-to-digital converter," *IEEE Sensors J.*, vol. 15, no. 7, pp. 3893–3902, Jul. 2015.

[19] J. O'Dowd, A. Callanan, G. Banarie, and E. Company-Bosch, "Capacitive sensor interfacing using sigma-delta techniques," in *Proc. IEEE Sensors*, Irvine, CA, USA, Oct./Nov. 2005, pp. 951–954.

[20] K. Lasanen and J. Kostamovaara, "A 1.2-V CMOS *RC* oscillator for capacitive and resistive sensor applications," *IEEE Trans. Instrum. Meas.*, vol. 57, no. 12, pp. 2792–2800, Dec. 2008.

[21] J.-S. An, S.-K. Hong, and O.-K. Kwon, "A highly linear and accurate touch data extraction algorithm based on polar coordinates for large-sized capacitive touch screen panels," *IEEE Trans. Consum. Electron.*, vol. 62, no. 4, pp. 341–348, Nov. 2016.

[22] K. Lim, K.-S. Jung, C.-S. Jang, J.-S. Baek, and I.-B. Kang, "A fast and energy efficient single-chip touch controller for tablet touch applications," *J. Display Technol.*, vol. 9, no. 7, pp. 520–526, Jul. 2013.

[23] S. Ko, H. Shin, H. Jang, I. Yun, and K. Lee, "A 70 dB SNR capacitive touch screen panel readout IC using capacitor-less trans-impedance amplifier and coded orthogonal frequency-division multiple sensing scheme," in *Proc. Symp. VLSI Circuits*, Kyoto, Japan, Jun. 2013, pp. C216–C217.

[24] S. Tsuji and T. Kohama, "A layered 3D touch screen using capacitance measurement," *IEEE Sensors J.*, vol. 14, no. 9, pp. 3040–3045, Sep. 2014.

[25] C. Brown, A. Kay, Y. Sugita, and K. Kita, "A capacitive touch panel for simultaneous detection of non-conductive and conductive objects," in *Soc. Inf. Display (SID) Symp. Dig.*, 2015, pp. 891–894.

[26] C. L. Lin, Y. M. Chang, C. C. Hung, C. D. Tu, and C. Y. Chuang, "Position estimation and smooth tracking with a fuzzy-logic-based adaptive strong tracking Kalman filter for capacitive touch panels," *IEEE Trans. Ind. Electron.*, vol. 62, no. 8, pp. 5097–5108, Aug. 2015.

[27] A. Yamada *et al.*, "A multi-core architecture of digital back-end for large mutual capacitance touch sensing systems," in *Proc. IEEE Int. Symp. Circuits Syst. (ISCAS)*, Lisbon, Portugal, May 2015, pp. 1382–1385.

[28] S. Gao, J. Lai, and A. Nathan, "Fast readout and low power consumption in capacitive touch screen panel by downsampling," *J. Display Technol.*, vol. 12, no. 11, pp. 1417–1422, Nov. 2016.

[29] H. S. Kim and K. Y. Han, "High-SNR capacitive multi-touch sensing technique for AMOLED display panels," *IEEE Sensors J.*, vol. 16, no. 4, pp. 859–860, Feb. 2016.

[30] B. Li, T. Wei, X. Wei, J. Wang, W. Liu, and R. Zheng, "A touch prediction and window sensing strategy for low-power and low-cost capacitive multitouch screen systems," *J. Display Technol.*, vol. 12, no. 6, pp. 646–657, Jun. 2016.

[31] H. Lim, Y. Jun, S. Han, S. Ha, Y. Jung, and S. Lee, "Implementation of a touch screen panel with triangle twist sensor pattern and controller IC," *J. Display Technol.*, vol. 12, no. 10, pp. 1218–1223, Oct. 2016.

[32] Y.-H. Yu and T.-Y. Sun, "A pseudo-differential measuring approach for implementing microcontroller-based capacitive touch sensing in low-power quality situation," *IEEE Sensors J.*, vol. 16, no. 2, pp. 390–399, Jan. 2016.

[33] H. Akhtar, Q. Kemao, and R. Kakarala, "A review of sensing technologies for small and large-scale touch panels," in *Proc. SPIE*, vol. 10449, pp. 1044918-1–1044918-13, Jun. 2017.

[34] Y. Huh *et al.*, "A 10.1" 56-channel, 183 uW/electrode, 0.73 mm^2/sensor high SNR 3D hover sensor based on enhanced signal refining and fine error calibrating techniques," in *Proc. Symp. VLSI Circuits*, Kyoto, Japan, Jun. 2017, pp. C308–C309.

[35] C. B. Thoresen and U. Hanke, "Numerical simulation of mutual capacitance touch screens for ungrounded objects," *IEEE Sensors J.*, vol. 17, no. 16, pp. 5143–5152, Aug. 2017.

[36] J.-H. Jun, B.-J. Kim, S.-K. Shin, K. Jang, J.-S. Baek, and C. Kim, "In-cell self-capacitive-type mobile touch system and embedded readout circuit in display driver IC," *IEEE J. Display Technol.*, vol. 12, no. 12, pp. 1613–1622, Dec. 2016.

[37] G. Walker. (Jun. 2014). *Fundamentals of Projected-Capacitive Touch Technology*. Accessed: May 5, 2018. [Online] Available: http://walkermobile.com/Touch_Technologies_Tutorial_Latest_Version.pdf

[38] M. Miyamoto, "How to realize high SNR projected capacitive touch systems with very large format," in *Proc. Int. Display Workshop*, 2013, pp. 1630–1633.

[39] S. P. Hotelling, M. Yousefpor, S. C. Chang, and J. Z. Zhong, "Integrated touch screen," U.S. Patent 7 859 521 B2, Dec. 28, 2010.

[40] S. P. Hotelling and J. Z. Zhong, "Integrated in-plane switching display and touch sensor," U.S. Patent 8 040 326 B2, Oct. 18, 2011.

[41] S. P. Hotelling, M. Yousefpor, S. C. Chang, and J. Z. Zhong, "Integrated touch screen," U.S. Patent 2013/0 176 281 A1, Jul. 11, 2013.

[42] S. P. Hotelling, C. H. Krah, and B. Q. Huppi, "Multipoint touch surface controller," U.S. Patent 2007/0 257 890 A1, Nov. 8, 2007.

[43] S. P. Hotelling, J. A. Strickon, and B. Q. Huppi, "Multipoint touch-screen," U.S. Patent 7 663 607 B2, Feb. 16, 2010.

[44] T.-H. Hwang, W.-H. Cui, I.-S. Yang, and O.-K. Kwon, "A highly area-efficient controller for capacitive touch screen panel systems," *IEEE Trans. Consum. Electron.*, vol. 56, no. 2, pp. 1115–1122, May 2010.

[45] S. Ko *et al.*, "Low noise capacitive sensor for multi-touch mobile handset's applications," in *Proc. IEEE Asian Solid-State Circuits Conf.*, Beijing, China, Nov. 2010, pp. 1–4.

[46] K.-D. Kim *et al.*, "A capacitive touch controller robust to display noise for ultrathin touch screen displays," in *IEEE Int. Solid-State Circuits Conf. (ISSCC) Dig. Tech. Papers*, San Francisco, CA, USA, Feb. 2012, pp. 116–117.

[47] H. K. Ouh, J. Lee, S. Han, H. Kim, I. Yoon, and S. Hong, "A programmable mutual capacitance sensing circuit for a large-sized touch panel," in *Proc. IEEE Int. Symp. Circuits Syst.*, Seoul, South Korea, May 2012, pp. 1395–1398.

[48] M. G. A. Mohamed, K. Cho, and H. Kim, "Frequency selection concurrent sensing technique for high-performance touch screens," *J. Display Technol.*, vol. 12, no. 11, pp. 1433–1443, Nov. 2016.

[49] J.-S. An *et al.*, "A 3.9 kHz-frame-rate capacitive touch system with pressure/tilt angle expressions of active stylus using multiple-frequency driving method for 65" 104×64 touch screen panel," in *IEEE Int. Solid-State Circuits Conf. (ISSCC) Dig. Tech. Papers*, San Francisco, CA, USA, Feb. 2017, pp. 168–169.

[50] C. Kim *et al.*, "Advanced in-cell touch technology for large sized liquid crystal displays," in *Soc. Inf. Display (SID) Symp. Dig.*, May 2015, vol. 46. no. 1, pp. 895–898.

[51] I. S. Yang and O. K. Kwon, "A touch controller using differential sensing method for on-cell capacitive touch screen panel systems," *IEEE Trans. Consum. Electron.*, vol. 57, no. 3, pp. 1027–1032, Aug. 2011.

[52] J.-H. Yang *et al.*, "A high-SNR area-efficient readout circuit using a delta-integration method for capacitive touch screen panels," in *SID Symp. Dig. Tech. Papers*, 2012, pp. 1570–1573.

[53] H. Shin, S. Ko, H. Jang, I. Yun, and K. Lee, "A 55 dB SNR with 240 Hz frame scan rate mutual capacitor 30×24 touch-screen panel read-out IC using code-division multiple sensing technique," in *IEEE Int. Solid-State Circuits Conf. (ISSCC) Dig. Tech. Papers*, San Francisco, CA, USA, Feb. 2013, pp. 388–389.

[54] J.-H. Yang *et al.*, "A highly noise-immune touch controller using filtered-delta-integration and a charge-interpolation technique for 10.1-inch capacitive touch-screen panels," in *IEEE Int. Solid-State Circuits Conf. (ISSCC) Dig. Tech. Papers*, San Francisco, CA, USA, Feb. 2013, pp. 390–391.

[55] J.-H. Yang, S.-C. Jung, Y.-S. Son, S.-T. Ryu, and G.-H. Cho, "A noise-immune high-speed readout circuit for in-cell touch screen panels," *IEEE Trans. Circuits Syst. I, Reg. Papers*, vol. 60, no. 7, pp. 1800–1809, Jul. 2013.

[56] M. Hamaguchi, A. Nagao, and M. Miyamoto, "A 240 Hz-reporting-rate 143×81 mutual-capacitance touch-sensing analog front-end IC with 37 dB SNR for 1 mm-diameter stylus," in *IEEE Int. Solid-State Circuits Conf. (ISSCC) Dig. Tech. Papers*, San Francisco, CA, USA, Feb. 2014, pp. 214–215.

[57] M. Miyamoto, M. Hamaguchi, and A. Nagao, "A 143×81 mutual-capacitance touch-sensing analog front-end with parallel drive and differential sensing architecture," *IEEE J. Solid-State Circuits*, vol. 50, no. 1, pp. 335–343, Jan. 2015.

[58] J.-E. Park, D.-H. Lim, and D.-K. Jeong, "A reconfigurable 40-to-67 dB SNR, 50-to-6400 Hz frame-rate, column-parallel readout IC for capacitive touch-screen panels," *IEEE J. Solid-State Circuits*, vol. 49, no. 10, pp. 2305–2318, Oct. 2014.

[59] K.-D. Kim *et al.*, "A fully-differential capacitive touch controller with input common-mode feedback for symmetric display noise cancellation," in *Symp. VLSI Circuits Dig. Tech. Papers*, Honolulu, HI, USA, Jun. 2014, pp. 1–2.

[60] Y.-S. Jang, Y.-H. Ko, J.-M. Choi, H.-S. Oh, and S.-G. Lee, "A 45-dB, 150-Hz, and 18-mW touch controller for on-cell capacitive TSP systems," *IEEE Trans. Circuits Syst. II, Exp. Briefs*, vol. 61, no. 10, pp. 748–752, Oct. 2014.

[61] J. S. Lee, D.-H. Yeo, H.-J. Kwon, B. Kim, J.-Y. Sim, and H.-J. Park, "An LCD-VCOM-noise resilient mutual-capacitive touch-sensor IC chip with a low-voltage driving signal," *IEEE Sensors J.*, vol. 15, no. 8, pp. 4595–4602, Aug. 2015.

[62] S. Heo *et al.*, "72 dB SNR, 240 Hz frame rate readout IC with differential continuous-mode parallel architecture for larger touch-screen panel applications," *IEEE Trans. Circuits Syst. I, Reg. Papers*, vol. 63, no. 7, pp. 960–971, Jul. 2016.

[63] J.-E. Park, J. Park, Y.-H. Hwang, J. Oh, and D.-K. Jeong, "A 100-TRX-channel configurable 85-to-385Hz-frame-rate analog front-end for touch controller with highly enhanced noise immunity of $20V_{pp}$," *IEEE Int. Solid-State Circuits Conf. (ISSCC) Dig. Tech. Papers*, San Francisco, CA, USA, Jan./Feb. 2016, pp. 210–211.

[64] D.-H. Yeo, S.-H. Kim, H.-K. Noh, B. Kim, J.-Y. Sim, and H.-J. Park, "A SNR-enhanced mutual-capacitive touch-sensor ROIC using an averaging with three specific TX frequencies, a noise memory, and a compact delay compensation circuit," *IEEE Sensors J.*, vol. 16, no. 18, pp. 6931–6938, Sep. 2016.

[65] S.-H. Park, H.-S. Kim, J.-S. Bang, G.-H. Cho, and G.-H. Cho, "A 0.26-nJ/node, 400-kHz Tx driving, filtered fully differential readout IC with parasitic RC time delay reduction technique for 65-in 169×97 capacitive-type touch screen panel," *IEEE J. Solid-State Circuits*, vol. 52, no. 2, pp. 528–542, Feb. 2017.

[66] H. Hwang, H. Lee, M. Han, H. Kim, and Y. Chae, "A 1.8-V 6.9-mW 120-fps 50-channel capacitive touch readout with current conveyor AFE and current-driven $\Delta\Sigma$ ADC," *IEEE J. Solid-State Circuits*, vol. 53, no. 1, pp. 204–218, Jan. 2018.

[67] T. Denison, K. Consoer, W. Santa, A.-T. Avestruz, J. Cooley, and A. Kelly, "A 2 μW 100 nV/rtHz chopper-stabilized instrumentation amplifier for chronic measurement of neural field potentials," *IEEE J. Solid-State Circuits*, vol. 42, no. 12, pp. 2934–2945, Dec. 2007.

[68] N. Verma, A. Shoeb, J. Bohorquez, J. Dawson, J. Guttag, and A. P. Chandrakasan, "A micro-power EEG acquisition SoC with integrated feature extraction processor for a chronic seizure detection system," *IEEE J. Solid-State Circuits*, vol. 45, no. 4, pp. 804–816, Apr. 2010.

[69] K.-D. Kim *et al.*, "A capacitive touchscreen controller IC with noise-based hybrid sensing scheme," in *SID Symp. Dig. Tech. Papers*, 2013, pp. 626–629.

[70] N. Miura *et al.*, "A 1 mm-pitch 80×80-channel 322 Hz-frame-rate touch sensor with two-step dual-mode capacitance scan," in *IEEE Int. Solid-State Circuits Conf. (ISSCC) Dig. Tech. Papers*, San Francisco, CA, USA, Feb. 2014, pp. 216–217.

[71] J.-S. An, S.-J. Jung, S.-K. Hong, and O.-K. Kwon, "A highly noise-immune capacitive touch sensing system using an adaptive chopper stabilization method," *IEEE Sensors J.*, vol. 17, no. 3, pp. 803–811, Feb. 2017.

[72] R. R. Schediwy and F. Faggin, "Finger/stylus touch pad," U.S. Patent 8 089 470 B1, Jan. 3, 2012.

[73] *Wacom EMR Technology*. Accessed: Apr. 3, 2018. [Online]. Available: https://www.wacom.com/en-us/products/smartpads/bamboo-folio

[74] *Dessecting the Galaxy Note-Take a Look Inside*. Accessed: Apr. 3, 2018. [Online]. Available: https://news.samsung.com/global/dissecting-the-galaxy-note-take-a-look-inside

[75] *S Pen for Galaxy Tab S3 and Galaxy Book*. Accessed: Apr. 3, 2018. [Online]. Available: http://www.samsung.com/uk/business/mobile-accessories/s-pen-pp355-galaxy-tab-a-9-7/

[76] H. Hara, "Position detector and position pointer," U.S. Patent 2015/0 338 930 A1, Nov. 26, 2015.

[77] C. Park *et al.*, "A pen-pressure-sensitive capacitive touch system using electrically coupled resonance pen," in *IEEE Int. Solid-State Circuits Conf. (ISSCC) Dig. Tech. Papers*, San Francisco, CA, USA, Feb. 2015, pp. 1–3.

[78] C. Park *et al.*, "A pen-pressure-sensitive capacitive touch system using electrically coupled resonance pen," *IEEE J. Solid-State Circuits*, vol. 51, no. 1, pp. 168–176, Jan. 2016.

[79] K.-H. Lee *et al.*, "A noise-immune stylus analog front-end using adjustable frequency modulation and linear-interpolating data reconstruction for both electrically coupled resonance and active styluses," in *IEEE Int. Solid-State Circuits Conf. (ISSCC) Dig. Tech. Papers*, San Francisco, CA, USA, Feb. 2018, pp. 184–185.

[80] *Microsoft Surface Pen*. Accessed: Feb. 2, 2018. [Online]. Available: https://www.microsoft.com/surface/en-us/accessories/pen

[81] V. K. Bakken, E. Yilmaz, and S. Shahparnia, "Active-stylus nib with rolling-ball tip," U.S. Patent 2013/0 106 771 A1, May 2, 2013.

[82] S. Shahparnia *et al.*, "Pulse- or frame-based communication using active stylus," U.S. Patent 9 280 220 B2, Mar. 8, 2016.

[83] K. Sundara-Rajan and S. Shahparnia, "Multi-electrode active stylus tip," U.S. Patent 2013/0 106 717 A1, May 2, 2013.

[84] M. Agarwal, S. Shahparnia, and M. P. Grunthaner, "Noise correction for stylus applications on tablets and other touch devices," U.S. Patent 2014/0 152 582 A1, Jun. 5, 2014.

[85] J. A. Harley, L.-Q. Tan, D. Mukherjee, and S. P. Hotelling, "Stylus orientation detection," U.S. Patent 8 638 320 B2, Jan. 28, 2014.

[86] C. H. Krah, S. Shahparnia, and S. P. Hotelling, "Input device for touch sensitive devices," U.S. Patent 2014/0 028 577 A1, Jan. 30, 2014.

[87] S. Shahparnia, "Input device for and method of communication with capacitive devices through frequency variation," U.S. Patent 2014/0 028 576 A1, Jan. 30, 2014.

[88] M. Agarwal, S. S. Shahparnia, and V. Pant, "Noise reduction for touch sensor system with active stylus," U.S. Patent 2016/0 147 319 A1, May 26, 2016.

[89] S. Shahparnia, C. T. Mullens, M. P. Grunthaner, and A. Geboff, "Coarse scan and targeted active mode scan for touch," U.S. Patent 2016/0 162 101 A1, Jun. 9, 2016.

[90] M. Hamaguchi, M. Takeda, and M. Miyamoto, "A 240 Hz-reporting-rate mutual-capacitance touch-sensing analog front-end enabling multiple active/passive styluses with 41 dB/32 dB SNR for 0.5 mm diameter," in *IEEE Int. Solid-State Circuits Conf. (ISSCC) Dig. Tech. Papers*, San Francisco, CA, USA, Feb. 2015, pp. 1–3.

[91] J.-S. An *et al.*, "A 3.9-kHz frame rate and 61.0-dB SNR analog front-end IC with 6-bit pressure and tilt angle expressions of active stylus using multiple-frequency driving method for capacitive touch screen panels," *IEEE J. Solid-State Circuits*, vol. 53, no. 1, pp. 187–203, Jan. 2018.

[92] S.-I. Yoshida, M. Hamaguchi, T. Morishita, S. Shinjo, A. Nagao, and M. Miyamoto, "An 87×49 mutual capacitance touch sensing IC enabling 0.5 mm-diameter stylus signal detection at 240 Hz-reporting-rate with palm rejection," in *Proc. IEEE Asian Solid-State Circuits Conf. (A-SSCC)*, KaoHsiung, Taiwan, Nov. 2014, pp. 217–220.

[93] J.-S. An *et al.*, "Multi-way interactive capacitive touch system with palm rejection of active stylus for 86" touch screen panels," in *IEEE Int. Solid-State Circuits Conf. (ISSCC) Dig. Tech. Papers*, San Francisco, CA, USA, Feb. 2018, pp. 182–183.

[94] I. Geller, U. Ron, and A. Peretz, "Stylus synchronization with a digitizer system," U.S. Patent 2016/0 209 940 A1, Jul. 21, 2016.

[95] M.-S. Shin, J.-B. Kim, M.-K. Kim, Y.-R. Jo, and O.-K. Kwon, "A 1.92-megapixel CMOS image sensor with column-parallel low-power and area-efficient SA-ADCs," *IEEE Trans. Electron Devices*, vol. 59, no. 6, pp. 1693–1700, Jun. 2012.

[96] M.-S. Shin *et al.*, "CMOS X-ray detector with column-parallel 14.3-bit extended-counting ADCs," *IEEE Trans. Electron Devices*, vol. 60, no. 3, pp. 1169–1177, Mar. 2013.

[97] M. K. Kim, S. K. Hong, and O. K. Kwon, "A small-area and energy-efficient 12-bit SA-ADC with residue sampling and digital calibration for CMOS image sensors," *IEEE Trans. Circuits Syst. II, Exp. Briefs*, vol. 62, no. 10, pp. 932–936, Oct. 2015.

[98] Y. R. Jo, S. K. Hong, and O. K. Kwon, "A low-noise and area-efficient PWM-$\Delta\Sigma$ ADC using a single-slope quantizer for CMOS image sensors," *IEEE Trans. Electron Devices*, vol. 63, no. 1, pp. 168–173, Jan. 2016.

[99] J.-W. Lee, D.-J. Min, J. Kim, and W. Kim, "A 600-dpi capacitive fingerprint sensor chip and image-synthesis technique," *IEEE J. Solid-State Circuits*, vol. 34, no. 4, pp. 469–475, Apr. 1999.

[100] S. Jung, R. Thewes, T. Scheiter, K. F. Goser, and W. Weber, "A low-power and high-performance CMOS fingerprint sensing and encoding architecture," *IEEE J. Solid-State Circuits*, vol. 34, no. 7, pp. 978–984, Jul. 1999.

[101] H. Morimura, S. Shigematsu, and K. Machida, "A novel sensor cell architecture and sensing circuit scheme for capacitive fingerprint sensors," *IEEE J. Solid-State Circuits*, vol. 35, no. 5, pp. 724–731, May 2000.

[102] K. Machida *et al.*, "A novel semiconductor capacitive sensor for a single-chip fingerprint sensor/identifier LSI," *IEEE Trans. Electron Devices*, vol. 48, no. 10, pp. 2273–2278, Oct. 2001.

[103] H. Morimura, S. Shigematsu, T. Shimamura, K. Machida, and H. Kyuragi, "A pixel-level automatic calibration circuit scheme for capacitive fingerprint sensor LSIs," *IEEE J. Solid-State Circuits*, vol. 37, no. 10, pp. 1300–1306, Oct. 2002.

[104] O. Vermesan *et al.*, "A 500-dpi AC capacitive hybrid flip-chip CMOS ASIC/sensor module for fingerprint, navigation, and pointer detection with on-chip data processing," *IEEE J. Solid-State Circuits*, vol. 38, no. 12, pp. 2288–2296, Dec. 2003.

[105] R. Hashido, A. Suzuki, A. Iwata, T. Okamoto, Y. Satoh, and M. Inoue, "A capacitive fingerprint sensor chip using low-temperature poly-Si TFTs on a glass substrate and a novel and unique sensing method," *IEEE J. Solid-State Circuits*, vol. 38, no. 2, pp. 274–280, Feb. 2003.

[106] S.-M. Jung, J.-M. Nam, D.-H. Yang, and M.-K. Lee, "A CMOS integrated capacitive fingerprint sensor with 32-bit RISC microcontroller," *IEEE J. Solid-State Circuits*, vol. 40, no. 8, pp. 1745–1750, Aug. 2005.

[107] S. J. Kim, K. H. Lee, S. W. Han, and E. Yoon, "A CMOS fingerprint system-on-a-chip with adaptable pixel networks and column-parallel processors for image enhancement and recognition," *IEEE J. Solid-State Circuits*, vol. 43, no. 11, pp. 2558–2567, Nov. 2008.

[108] T. Shimamura, H. Morimura, S. Shigematsu, M. Nakanishi, and K. Machida, "Capacitive-sensing circuit technique for image quality improvement on fingerprint sensor LSIs," *IEEE J. Solid-State Circuits*, vol. 45, no. 5, pp. 1080–1087, May 2010.

[109] J.-C. Liu, Y.-S. Hsiung, and M. S.-C. Lu, "A CMOS micromachined capacitive sensor array for fingerprint detection," *IEEE Sensors J.*, vol. 12, no. 5, pp. 1004–1010, May 2012.

[110] T. Shimamura *et al.*, "Impedance-sensing circuit techniques for integration of a fraud detection function into a capacitive fingerprint sensor," *IEEE Sensors J.*, vol. 12, no. 5, pp. 1393–1401, May 2012.

[111] H. Ma *et al.*, "On-display transparent half-diamond pattern capacitive fingerprint sensor compatible with AMOLED display," *IEEE Sensors J.*, vol. 16, no. 22, pp. 8124–8131, Nov. 2016.

[112] S.-H. Lee, J.-S. An, S.-K. Hong, and O.-K. Kwon, "In-cell capacitive touch panel structures and their readout circuits," in *Proc. 23rd Int. Workshop Active-Matrix Flatpanel Displays Devices (AM-FPD)*, Kyoto, Japan, Jul. 2016, pp. 258–261.

[113] Y.-K. Choi *et al.*, "An integrated LDI with readout function for touch-sensor-embedded display panels," in *IEEE Int. Solid-State Circuits Conf. (ISSCC) Dig. Tech. Papers*, San Francisco, CA, USA, Feb. 2007, pp. 134–135.
[114] H.-R. Kim *et al.*, "A mobile-display-driver IC embedding a capacitive-touch-screen controller system," in *IEEE ISSCC Dig. Tech. Papers*, San Francisco, CA, USA, Feb. 2010, pp. 114–115.
[115] M. Ozbas, I. Knausz, J. Lillie, C. Ludden, T. Mackin, and D. Gillespie, "An in-cell capable capacitive touchscreen controller with high SNR and integrated display driver IC for WVGA LTPS displays," in *SID Symp. Dig. Tech. Papers*, 2012, pp. 485–488.
[116] C.-L. Lin, C.-S. Li, Y.-M. Chang, Y.-C. Hung, and A. Lin, "3D stylus and pressure sensing system for capacitive touch panel," in *Proc. IEEE Int. Conf. Consum. Electron. (ICCE)*, Las Vegas, NV, USA, Jan. 2012, pp. 215–216.
[117] K. Reynolds, P. Shepelev, and A. Graf, "Touch and display integration with force," in *SID Symp. Dig. Tech. Papers*, 2016, pp. 617–620.
[118] Samsung. *Galaxy S8*. Accessed: Feb. 2, 2018 [Online]. Available: http://www.samsung.com/global/galaxy/galaxy-s8/specs/
[119] Y. Visell, A. Law, and J. R. Cooperstock, "Touch is everywhere: Floor surfaces as ambient haptic interfaces," *IEEE Trans. Haptics*, vol. 2, no. 3, pp. 148–159, Jul./Sep. 2009.
[120] T. Yoshikawa and A. Nagura, "A touch/force display system for haptic interface," *Presence*, vol. 10, no. 2, pp. 225–235, Apr. 2001.
[121] H. Nagano, S. Okamoto, and Y. Yamada, "Haptic invitation of textures: Perceptually prominent properties of materials determine human touch motions," *IEEE Trans. Haptics*, vol. 7, no. 3, pp. 345–355, Jul./Sep. 2014.
[122] D. J. Tyler, "Restoring the human touch: Prosthetics imbued with haptics give their wearers fine motor control and a sense of connection," *IEEE Spectr.*, vol. 53, no. 5, pp. 28–33, May 2016.
[123] M. A. Eid and H. Al Osman, "Affective haptics: Current research and future directions," *IEEE Access*, vol. 4, pp. 26–40, 2016.
[124] G. Huisman, "Social touch technology: A survey of haptic technology for social touch," *IEEE Trans. Haptics*, vol. 10, no. 3, pp. 391–408, Jul./Sep. 2017.
[125] F. Beruscha, W. Krautter, A. Lahmer, and M. Pauly, "An evaluation of the influence of haptic feedback on gaze behavior during in-car interaction with touch screens," in *Proc. IEEE World Haptics Conf. (WHC)*, Munich, Germany, Jun. 2017, pp. 201–206.
[126] D. P. Heyman, A. Tabatabai, and T. V. Lakshman, "Statistical analysis and simulation study of video teleconference traffic in ATM networks," *IEEE Trans. Circuits Syst. Video Technol.*, vol. 2, no. 1, pp. 49–59, Mar. 1992.
[127] K.-F. Hwang and C.-C. Chang, "A self-encryption mechanism for authentication of roaming and teleconference services," *IEEE Trans. Wireless Commun.*, vol. 2, no. 2, pp. 400–407, Mar. 2003.
[128] D. G. Steer and L. Strawczynski, "A secure audio teleconference system," in *Proc. Conf. Rec. 21st Century Military Commun.-What's Possible? IEEE Military Commun. Conf. (MILCOM)*, vol. 1. San Diego, CA, USA, Oct. 1988, pp. 63–67.
[129] C. Liu, Y. Xie, M. J. Lee, and T. N. Saadawi, "Multipoint multimedia teleconference system with adaptive synchronization," *IEEE J. Sel. Areas Commun.*, vol. 14, no. 7, pp. 1422–1435, Sep. 1996.
[130] *Digital Stationary Consortium*. Accessed: Feb. 2, 2018. [Online]. Available: https://digitalstationeryconsortium.org

Oh-Kyong Kwon (S'83–M'88) received the B.S. degree in electronic engineering from Hanyang University, Seoul, South Korea, in 1978, and the M.S. and Ph.D. degrees in electrical engineering from Stanford University, Stanford, CA, USA, in 1986 and 1988, respectively.

From 1987 to 1992, he was with the Semiconductor Process and Design Center, Texas Instruments Inc., Dallas, TX, USA, where he was engaged in the development of multichip module technologies and smart power integrated circuit technologies for automotive and flat panel display applications. In 1992, he joined Hanyang University, Seoul, South Korea, as an Assistant Professor with the Department of Electronic Engineering, where he is currently a Professor. He has authored or co-authored over 363 international journal and conference papers and holds 219 U.S. patents. His research interests include driving and sensing schemes for capacitive touch sensing system with passive and active styli, information display electronics, mixed mode signal circuit design, imager, analog front-end circuit design for bio-medical instruments, interconnect and electrical noise modeling for high-speed system-level integration, wafer-scale chip-size packages, and smart power integrated circuit technologies.

Jae-Sung An (S'12) received the B.S. degree in media communications engineering from Hanyang University, Seoul, South Korea, in 2010, where he is currently pursuing the Ph.D. degree in electronics and computer engineering. His research interests include high-precision analog integrated circuit design, driving and sensing schemes for capacitive touch systems with passive and active styli, and fingerprint sensing systems. Capacitive touch systems with multi-functional active stylus, which were designed by him, are announced in two IEEE ISSCC presentations and demonstrations from 2017 to 2018.

Seong-Kwan Hong (M'13) received the B.S. degree in electronic engineering from Hanyang University, Seoul, South Korea, in 1980, and the M.S. and Ph.D. degrees in electrical engineering from the Georgia Institute of Technology, Atlanta, GA, USA, in 1985 and 1994, respectively. From 1990 to 1995, he was with Cadence Design Systems Inc., San Jose, CA, USA, where he developed several ECAD products. In 1995, he joined the Research and Development Laboratory of LG Semicon, Seoul, South Korea, where he was in charge of the Design Technology Center as a Research Fellow. In 1999, he became a Vice President and Chief Information Officer at Hynix Semiconductor Inc., where he was responsible for information technology and Research and Development engineering support. From 2009 to 2013, he was with Yonsei University, Seoul, South Korea, as a Hynix Chair and a Research Professor. In 2013, he joined Hanyang University as a Research Professor. His research interests are EDA design methodology, mixed IC design, and automotive IC design.